

# Selective Gas Uptake and Rotational Dynamics in a (3,24)-Connected Metal–Organic Framework Material

William J. F. Trenholme, Daniil I. Kolokolov,\* Michelle Bound, Stephen P. Argent, Jamie A. Gould, Jiangnan Li, Sarah A. Barnett, Alexander J. Blake, Alexander G. Stepanov, Elena Besley, Timothy L. Easun,\* Sihai Yang,\* and Martin Schröder\*

Cite This: *J. Am. Chem. Soc.* 2021, 143, 3348–3358

Read Online

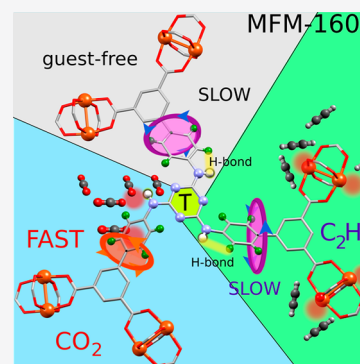
ACCESS |

Metrics & More

Article Recommendations

Supporting Information

**ABSTRACT:** The desolvated (3,24)-connected metal–organic framework (MOF) material, MFM-160a,  $[\text{Cu}_3(\text{L})(\text{H}_2\text{O})_3]$  [ $\text{H}_6\text{L}$  = 1,3,5-triazine-2,4,6-tris(aminophenyl-4-isophthalic acid)], exhibits excellent high-pressure uptake of  $\text{CO}_2$  (110 wt% at 20 bar, 298 K) and highly selective separation of  $\text{C}_2$  hydrocarbons from  $\text{CH}_4$  at 1 bar pressure. Henry's law selectivities of 79:1 for  $\text{C}_2\text{H}_2:\text{CH}_4$  and 70:1 for  $\text{C}_2\text{H}_4:\text{CH}_4$  at 298 K are observed, consistent with ideal adsorption solution theory (IAST) predictions. Significantly, MFM-160a shows a selectivity of 16:1 for  $\text{C}_2\text{H}_2:\text{CO}_2$ . Solid-state  $^2\text{H}$  NMR spectroscopic studies on partially deuterated MFM-160- $d_{12}$  confirm an ultra-low barrier ( $\sim 2$  kJ mol $^{-1}$ ) to rotation of the phenyl group in the activated MOF and a rotation rate 5 orders of magnitude slower than usually observed for solid-state materials ( $1.4 \times 10^6$  Hz cf.  $10^{11}$ – $10^{13}$  Hz). Upon introduction of  $\text{CO}_2$  or  $\text{C}_2\text{H}_2$  into desolvated MFM-160a, this rate of rotation was found to increase with increasing gas pressure, a phenomenon attributed to the weakening of an intramolecular hydrogen bond in the triazine-containing linker upon gas binding. DFT calculations of binding energies and interactions of  $\text{CO}_2$  and  $\text{C}_2\text{H}_2$  around the triazine core are entirely consistent with the  $^2\text{H}$  NMR spectroscopic observations.



## INTRODUCTION

Over the past two decades there has been a great deal of interest in metal–organic framework (MOF) materials capable of selectively storing and separating gases. Two areas of significant interest are the capture of  $\text{CO}_2$ <sup>1–8</sup> and the separation of  $\text{C}_2$  hydrocarbons from methane.<sup>9–15</sup>  $\text{CO}_2$  is well-established as a leading contributor to climate change, and over 85% of the world's energy demand involves the burning of fossil fuels.<sup>16,17</sup> Materials capable of storing  $\text{CO}_2$  from flue gas and automobiles are therefore in high demand. The use of MOFs containing polar functional groups such as amines and amides has proven to be effective for the uptake of  $\text{CO}_2$  at low pressure, while MOFs with very large surface areas have shown exceptional storage capacity for  $\text{CO}_2$  at higher pressures.<sup>5,18–21</sup>

Natural gas is a vitally important fuel and is also a feedstock for the production of a variety of chemicals.<sup>22</sup> Comprised mainly of  $\text{CH}_4$ , it is also increasingly being utilized in vehicles, as its high H:C ratio results in lowered emissions of CO and  $\text{CO}_2$  compared to normal hydrocarbon fuels.<sup>22</sup> The main sources of impurity in natural gas are the  $\text{C}_2$  hydrocarbons,  $\text{C}_2\text{H}_2$ ,  $\text{C}_2\text{H}_4$ , and  $\text{C}_2\text{H}_6$ .<sup>11</sup> Removing these hydrocarbons increases the purity of natural gas and provides a source of  $\text{C}_2$  hydrocarbons for further use.<sup>23,24</sup> Purification and separation of  $\text{C}_2$  hydrocarbons are usually achieved by cryogenic distillation, a very energy-intensive process, and the use of selective adsorbents to separate different components at room temperature is a potential alternative.<sup>23,24</sup>

We report herein the synthesis of the hexacarboxylate linker  $\text{H}_6\text{L}$ , which has been used to prepare a (3,24)-connected Cu(II) material (denoted MFM-160; MFM = Manchester Framework Material) designed for both high  $\text{CO}_2$  uptake and selective sorption of  $\text{C}_2$  hydrocarbons over  $\text{CH}_4$ . With this in mind, our ligand design was based around a triazine core,<sup>11,23–26</sup> coupled with a triangular arrangement of three pendant isophthalic acid moieties, which can combine with a Cu(II) paddlewheel motif to give a framework of *rht* topology, used by us<sup>27–32</sup> and others<sup>33–35</sup> to prepare MOFs with exceptional gas storage capacity. We show here that MFM-160 has the potential for extremely high  $\text{CO}_2$  uptake at higher pressures, while at lower pressures it is capable of highly selective sorption of  $\text{C}_2$  hydrocarbons over  $\text{CH}_4$  and  $\text{CO}_2$ .

## EXPERIMENTAL SECTION

**Synthesis of  $\text{H}_6\text{L}$  (Scheme 1).** Cyanuric chloride (736 mg, 3.99 mmol) was added to a mixture of 4-bromoaniline (2.20 g, 12.8 mmol, 3.2 equiv) and  $\text{NaHCO}_3$  (1.08 g, 12.8 mmol, 3.2 equiv) in 1,4-dioxane/DMF (3:1, 30 mL) and the mixture heated at 120 °C in a

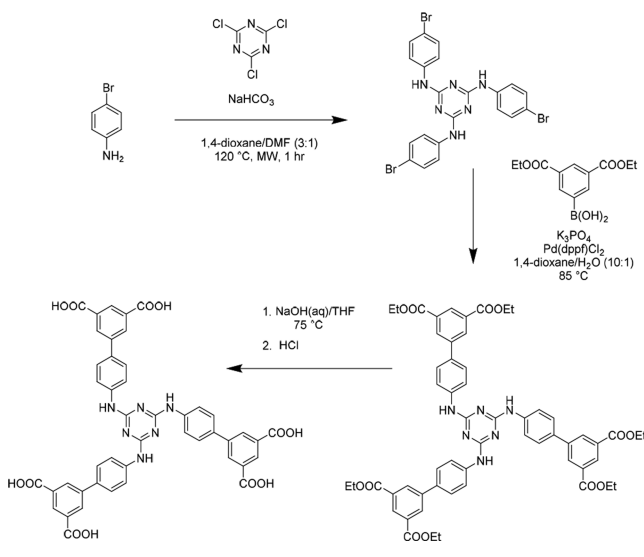
Received: October 24, 2020

Published: February 24, 2021



microwave reactor for 1 h. The solvent was removed under vacuum and the remaining solid washed with water (2 × 20 mL) and extracted into Et<sub>2</sub>O. The organic layer was separated and the solvent removed under vacuum. The resulting white solid was recrystallized from warm hexane:EtOAc (5:1), filtered, and dried to give 2,4,6-tris(4-bromophenylamino)-1,3,5-triazine (yield: 1.95 g, 83%). <sup>1</sup>H NMR spectroscopy (400 MHz, dms<sub>o</sub>-d<sub>6</sub>) δ = 9.54 (s, 3H), 7.80 (d, 6H, J = 6.8 Hz), 7.46 (d, 6H, J = 8.8 Hz); <sup>13</sup>C{<sup>1</sup>H} NMR (100 MHz, dms<sub>o</sub>-d<sub>6</sub>) δ = 164.3, 139.7, 131.6, 122.7, 114.2 ppm.

### Scheme 1. Synthesis of H<sub>6</sub>L



2,4,6-Tris(4-bromophenylamino)-1,3,5-triazine (1.32 g, 2.23 mmol), diethylisophthalate-5-boronic acid (2.14 g, 8.05 mmol, 3.6 equiv), and K<sub>3</sub>PO<sub>4</sub> (8.50 g, 40.1 mmol, 18 equiv) were added to a degassed mixture of 1,4-dioxane/water (10:1, 110 mL). [Pd(dppf)-Cl<sub>2</sub>] (40 mg, 0.055 mmol, 2.4% equiv) was added and the reaction heated in a microwave reactor at 85 °C for 1 h. The solvent was removed under vacuum and the product extracted into CHCl<sub>3</sub>. The combined organic phase was then washed with water and brine and dried over MgSO<sub>4</sub>. Upon evaporation of CHCl<sub>3</sub>, the crude product was dissolved in CH<sub>2</sub>Cl<sub>2</sub> and purified by passing through a plug of silica gel to give the pure ester product 1,3,5-triazine-2,4,6-tris(aminophenyl-4-isophthalic ethyl ester) as a white solid (yield: 1.86 g, 82%). <sup>1</sup>H NMR spectroscopy (300 MHz, dms<sub>o</sub>-d<sub>6</sub>) δ = 9.58 (s, 3H), 8.42 (t, 3H, J = 1.5 Hz), 8.39 (d, 6H, J = 1.5 Hz), 8.04 (d, 6H, J = 6.0 Hz), 7.71 (d, 6H, J = 8.7 Hz), 4.37 (q, 12H, J = 7.1 Hz), 1.35 (t, 18H, J = 7.1 Hz); <sup>13</sup>C{<sup>1</sup>H} NMR (100 MHz, dms<sub>o</sub>-d<sub>6</sub>) δ = 165.8, 165.1, 139.6, 138.6, 131.9, 131.5, 130.1, 129.8, 127.5, 121.4, 61.6, 14.6 ppm.

The hexa-ester (1.70 g, 1.67 mmol) was dissolved in a mixture of THF (30 mL) and 2 M NaOH (30 mL) and heated at 75 °C for 16 h. Upon cooling, THF (30 mL) was added, the aqueous layer was separated, and concentrated HCl was added dropwise to the solution until pH ~1. The resulting precipitate was filtered and recrystallized from a mixture of hot DMF/water (5:1) to give the H<sub>6</sub>L [1,3,5-triazine-2,4,6-tris(aminophenyl-4-isophthalic acid)] as a white solid (yield: 1.36 g, 96%). <sup>1</sup>H NMR (400 MHz, dms<sub>o</sub>-d<sub>6</sub>) δ = 9.59 (s, 3H), 8.44 (t, 3H, J = 1.6 Hz), 8.39 (d, 6H, J = 1.6 Hz), 8.04 (d, 6H, J = 8.0 Hz), 7.73 (d, 6H, J = 8.8 Hz); <sup>13</sup>C{<sup>1</sup>H} NMR (100 MHz, dms<sub>o</sub>-d<sub>6</sub>) δ = 167.1, 164.5, 141.4, 140.8, 132.6, 132.4, 131.3, 128.7, 127.5, 121.2 ppm. Anal. Calcd (Found) for C<sub>45</sub>H<sub>30</sub>N<sub>6</sub>O<sub>12</sub>: C, 63.83 (63.39); H, 3.57 (3.45); N, 9.93 (9.80)%.

**Synthesis of MFM-160·13DMF·7H<sub>2</sub>O.** H<sub>6</sub>L (100 mg, 0.118 mmol) and Cu(NO<sub>3</sub>)<sub>2</sub>·3H<sub>2</sub>O (114 mg, 0.472 mmol, 4 equiv) were added to DMF/H<sub>2</sub>O (8 mL; 15:1, v/v) and sonicated until dissolution. A solution of 3 M HNO<sub>3</sub> in DMF (3 mL) was then added and the solution heated in a 50 mL Schott bottle at 80 °C for

20 h. The crystalline product was removed by filtration, washed with copious hot DMF, and dried to yield a green powder (yield: 210 mg, 82%) Anal. Calcd (Found) for C<sub>84</sub>H<sub>135</sub>N<sub>19</sub>O<sub>35</sub>Cu<sub>3</sub>: C, 46.67 (46.28); H, 6.29 (6.23); N, 12.31 (12.42)%. Single crystals of MFM-160 were prepared on a small scale using 20 mg of H<sub>6</sub>L and 4 equiv of Cu(NO<sub>3</sub>)<sub>2</sub>·3H<sub>2</sub>O dissolved in DMF (1.5 mL). Addition of 3 M HNO<sub>3</sub> in DMF (0.6 mL) followed by heating in a sealed vial at 80 °C for 20 h produced green octahedral crystals suitable for single-crystal X-ray diffraction. The syntheses of H<sub>6</sub>L-d<sub>12</sub> and MFM-160-d<sub>12</sub> (Scheme 2) are described in the Supporting Information.

Density functional theory (DFT) calculations were performed as implemented in the Q-Chem quantum chemistry package.<sup>36</sup> The strength of adsorption sites was analyzed using a fragment of the linker formed by the central triazine ring and three phenyl rings (Figure S33). The binding energies (BE) between the guest molecule and the linker were calculated in addition to their relative positions corresponding to the strongest binding. These calculations were performed in two stages. Geometry optimization was carried out using dispersion-corrected DFT calculations at the B3LYP/6-31+G\*\* level of theory, and the binding energies were subsequently calculated at the higher B3LYP/6-311+G\*\* level, with BE = E<sub>opt</sub>(complex) - E<sub>opt</sub>(linker) - E<sub>opt</sub>(guest molecule). Binding energies were corrected for basis set superposition error (BSSE).

## RESULTS AND DISCUSSION

The preparation of H<sub>6</sub>L was achieved via microwave-assisted nucleophilic substitution between 4-bromoaniline and cyanuric chloride to give the tribromo intermediate (Scheme 1).<sup>37</sup> A microwave-assisted Pd(II)-catalyzed Suzuki cross-coupling of this intermediate with 3,5-di(ethoxycarbonyl)phenylboronic acid gave the hexa-ester product, which was then hydrolyzed in aqueous NaOH followed by acidification with HCl to give H<sub>6</sub>L in good yield. It is worth noting that the short reaction times of 1 h for each of the substitution and cross-coupling reactions provide a facile and energy-efficient route to this linker. Solvothermal reaction of H<sub>6</sub>L and Cu(NO<sub>3</sub>)<sub>2</sub>·3H<sub>2</sub>O in acidified DMF at 80 °C for 24 h yielded green octahedral single crystals of MFM-160, [Cu<sub>3</sub>(L)(H<sub>2</sub>O)<sub>3</sub>]<sub>3</sub>·13DMF·7H<sub>2</sub>O.

MFM-160 crystallizes in the tetragonal space group *I4/m* with unit cell dimensions *a* = 32.6838(3) Å, *c* = 48.0624(7) Å, and *V* = 51341(1) Å<sup>3</sup> and shows a (3,24)-connected framework structure of *rht* topology containing three distinct cages, A, B, and C (Figure 1). Cage A is a truncated cuboctahedron formed from 12 [Cu<sub>2</sub>(O<sub>2</sub>CR)<sub>4</sub>] paddlewheel units connected to 24 different linkers, with the spacing between cuboctahedra determined by the distance between isophthalate moieties on the arms of the linker. This results in the formation of larger cages B (truncated tetrahedron) and C (truncated cube). With the aqua ligands removed from the axial positions of the paddlewheel, the accessible internal diameter of cage A is 13.0 Å, and that of cage B is 13.8 Å, with a cage length of 22.7 Å and the accessible windows between these cages measuring 6.5–8.2 Å. The largest cage, C, has an accessible diameter of 19.6 Å and a cage length of 35.2 Å, with windows of 6.4–8.4 Å. All internal diameters were calculated by fitting a sphere from the center of the cage to its walls, taking into account van der Waals radii. Window diameters were calculated from the largest sphere able to fit through the aperture. The potential accessible volume of desolvated MFM-160a (“a” denotes the desolvated form) is 77%, as calculated by the VOID algorithm within the software PLATON<sup>38</sup> (after removal of all guest solvates and coordinated water molecules), with a calculated crystal density of 0.540 g cm<sup>-3</sup>. Thermogravimetric analysis of the as-synthesized sample of MFM-160 in air showed loss of DMF and H<sub>2</sub>O solvent below

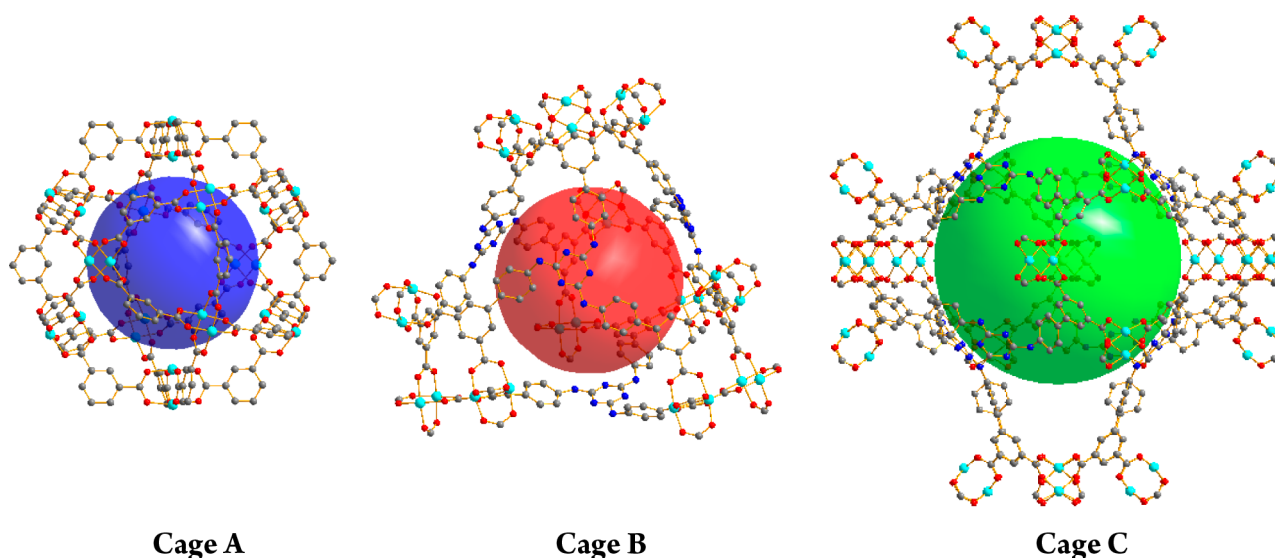


**Figure 1.** View of cages A, B, and C in MFM-160. The large colored spheres in the center of the cages represent the solvent-accessible volume. Color code for atoms: Cu, cyan; O, red; N, blue; C, gray. Hydrogen atoms are omitted for clarity.

170 °C, with the material stable up to 290 °C, above which a mass loss corresponding to framework decomposition is observed (Figure S2).

To prepare activated MFM-160a for gas sorption experiments, the DMF of the as-synthesized sample was exchanged with analytical-grade acetone by decanting the mother liquor and replacing it with analytical-grade acetone. This process was repeated twice daily for 5 days. The sample was then activated by heating at 100 °C under reduced pressure for 20 h, whereupon a color change from dark green to purple was observed; this is a typical indicator of the removal of coordinated solvent from the Cu(II) paddlewheel node. The permanent porosity of the framework was confirmed via a N<sub>2</sub> sorption isotherm measured volumetrically at 77 K, which showed reversible type-I behavior and an uptake of 983 cm<sup>3</sup> g<sup>-1</sup> (123 wt%) at 1 bar (Figure S5). The slight changes in gradient in the range 30–120 mbar are assigned to the sequential filling of the micropores and mesopores. The estimated Brunauer–Emmett–Teller (BET) surface area of MFM-160a as calculated from this isotherm was 3847 m<sup>2</sup> g<sup>-1</sup>, with a total pore volume of 1.52 cm<sup>3</sup> g<sup>-1</sup>.

#### CO<sub>2</sub>, H<sub>2</sub>, and Hydrocarbon Gas Adsorption Isotherms.

In order to probe the effectiveness of MFM-160a to adsorb different gases, we performed gas adsorption isotherm experiments between 0 and 20 bar using CO<sub>2</sub> and CH<sub>4</sub> (at 298 and 273 K, Figure 2) and H<sub>2</sub> (at 77 and 87 K, Figure S6). Low-pressure (0–1 bar) isotherms of C<sub>2</sub> hydrocarbons were run at 298 and 273 K for comparison with the data obtained for CH<sub>4</sub> (Figure 3).

MFM-160a shows exceptional capacity for CO<sub>2</sub> storage at 20 bar, with uptakes of 558 cm<sup>3</sup> g<sup>-1</sup> (110 wt%) and 719 cm<sup>3</sup> g<sup>-1</sup> (141 wt%) at 298 and 273 K, respectively. At 195 K and 1 bar, MFM-160a nears saturation at 881 cm<sup>3</sup> g<sup>-1</sup> (173 wt%). This uptake of CO<sub>2</sub> up to 20 bar at 298 K is one of the highest reported to date: to the best of our knowledge the current record uptake under these conditions is 627 cm<sup>3</sup> g<sup>-1</sup> (123 wt%, 19.8 bar) in MOF-177.<sup>5,20</sup> The CH<sub>4</sub> uptake of MFM-160a at 20 bar was 199 cm<sup>3</sup> g<sup>-1</sup> (14.2 wt%) at 298 K and 274 cm<sup>3</sup> g<sup>-1</sup> (19.6 wt%) at 273 K. The H<sub>2</sub> uptake at 20 bar was 6.4 wt% at

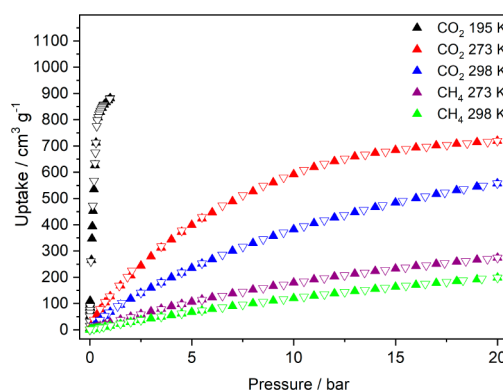


**Figure 2.** Adsorption isotherms for CO<sub>2</sub> and CH<sub>4</sub> in MFM-160a from 0 to 20 bar (filled triangles, adsorption; open triangles, desorption).

77 K and 5.3 wt% at 87 K, whereas the uptake at 1 bar was 2.14 wt% at 77 K and 1.40 wt% at 87 K (Figure S6).

As shown in Figure 3, the uptakes of C<sub>2</sub>H<sub>2</sub>, C<sub>2</sub>H<sub>4</sub>, and C<sub>2</sub>H<sub>6</sub> at 273 K are 212 cm<sup>3</sup> g<sup>-1</sup> (24.7 wt%), 175 cm<sup>3</sup> g<sup>-1</sup> (21.9 wt%), and 201 cm<sup>3</sup> g<sup>-1</sup> (27.0 wt%) at 1 bar, respectively. At 298 K, these values become 128 cm<sup>3</sup> g<sup>-1</sup> (14.9 wt%), 115 cm<sup>3</sup> g<sup>-1</sup> (14.4 wt%), and 110 cm<sup>3</sup> g<sup>-1</sup> (14.8 wt%). This comparatively low uptake of CH<sub>4</sub> at 1 bar (15.3 cm<sup>3</sup> g<sup>-1</sup> at 298 K, 27.1 cm<sup>3</sup> g<sup>-1</sup> at 273 K) in MFM-160a makes the material of great interest for selective separation of C<sub>2</sub> hydrocarbons over CH<sub>4</sub>. To estimate the selectivity of each hydrocarbon over CH<sub>4</sub>, we employed Henry's law, in which constants  $K_H$  were determined using a virial fit of the measured isotherm data (Figures S7–S16).

Using these constants, the selectivity ( $S$ ) of one gas,  $i$ , over the second gas,  $j$ , was determined from the following equation:

$$S_{ij} = K_{H_i}/K_{H_j}$$

The selectivities for C<sub>2</sub>H<sub>2</sub>:CH<sub>4</sub>, C<sub>2</sub>H<sub>4</sub>:CH<sub>4</sub>, and C<sub>2</sub>H<sub>6</sub>:CH<sub>4</sub> at 273 K were calculated to be 104:1, 130:1, and 10:1, respectively. While lower than current benchmark materials such as NKMOF-1-Ni<sup>39</sup> and ZJU-74a,<sup>40</sup> the C<sub>2</sub>H<sub>2</sub>:CH<sub>4</sub> separation of 79:1 at 298 K is comparable to those of other Cu(II) triazine-based MOFs, such as [Cu<sub>3</sub>(TDPAT)]<sup>11</sup>

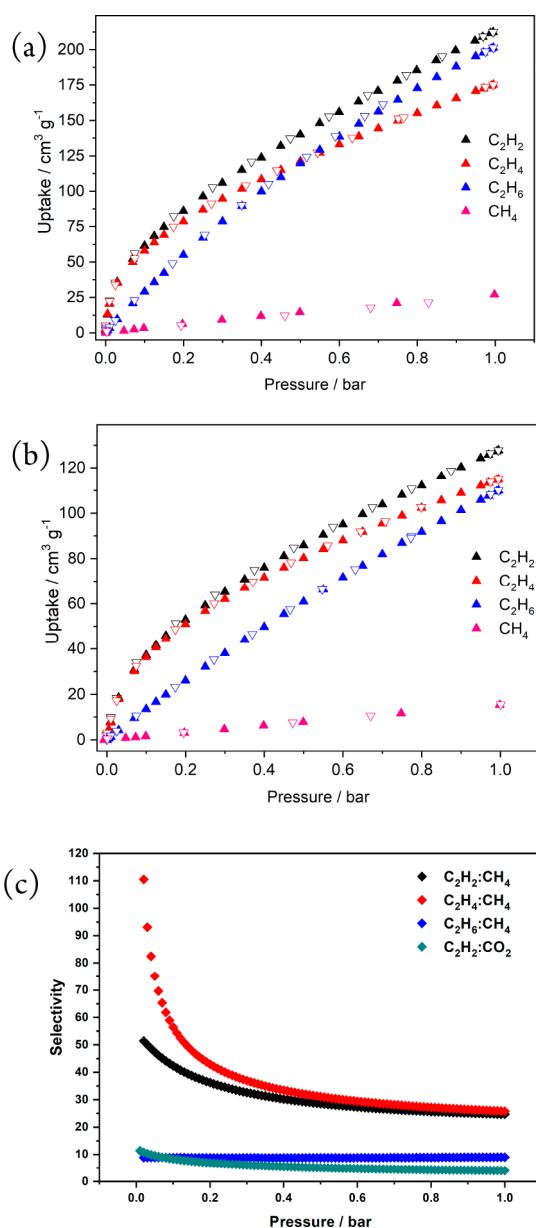


**Figure 3.** Adsorption isotherms for  $\text{CH}_4$ ,  $\text{C}_2\text{H}_6$ ,  $\text{C}_2\text{H}_4$ , and  $\text{C}_2\text{H}_2$  in MFM-160a from 0 to 1 bar at (a) 273 and (b) 298 K (filled triangles, adsorption; open triangles, desorption). (c) Calculated IAST selectivities for MFM-160a at 298 K.

(TDPAT<sup>6-</sup> = 2,4,6-tris(3,5-dicarboxylphenylamino)-1,3,5-triazine) and  $[\text{Cu}_3(\text{TDPAH})]^{23}$  (TDPAH<sup>6-</sup> = 2,5,8-tris(3,5-dicarboxylphenylamino)-*s*-heptazine), which have selectivities of 127:1 and 81:1, respectively. However, the calculated selectivities are higher than those reported for smaller-pore  $\text{Cu}(\text{II})$  MOFs such as UTSA-50a<sup>13</sup> and UTSA-15a<sup>41</sup> (68:1 and 56:1, respectively).

The selectivity for  $\text{C}_2\text{H}_2$  over  $\text{CO}_2$  (15:1 at 298 K; 16:1 at 273 K) demonstrates the potential of MFM-160a for the purification of acetylene, in which  $\text{CO}_2$  is a common impurity. A study by Li et al.<sup>42</sup> strongly suggested that the presence of N-centers within pores does not improve the selectivity for  $\text{C}_2\text{H}_2$  over  $\text{CO}_2$ . Thus, in the case of MFM-160a, we tentatively attribute this selectivity to the greater van der Waals interactions between the framework and  $\text{C}_2\text{H}_2$  molecules, as described by Samsonenko and co-workers for selective uptake

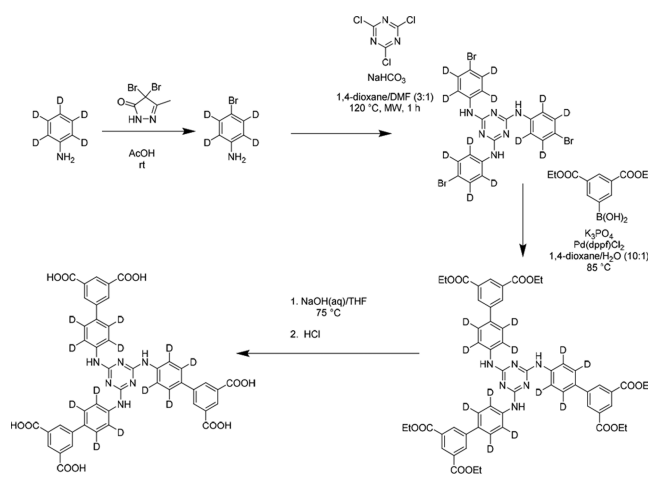
of  $\text{C}_2\text{H}_2$  over  $\text{CO}_2$  in porous formates.<sup>43</sup> The separation of  $\text{CO}_2$  from  $\text{C}_2\text{H}_2$  is notoriously difficult as a result of their similar sizes and sublimation points;<sup>44</sup> the current high selectivity for  $\text{C}_2\text{H}_2$  over  $\text{CO}_2$  is promising and represents one of the highest selectivities for a MOF for this separation.<sup>45,46</sup> It should be noted that repeating the desorption–adsorption cycles of these isotherms gives identical results, confirming the stability of MFM-160 to repeated activation and reuse.

In addition to Henry's law, the gas selectivities for  $\text{C}_2\text{H}_2:\text{CH}_4$ ,  $\text{C}_2\text{H}_4:\text{CH}_4$ ,  $\text{C}_2\text{H}_6:\text{CH}_4$ , and  $\text{C}_2\text{H}_2:\text{CO}_2$  in binary mixtures were analyzed using the ideal adsorption solution theory (IAST) model.<sup>47</sup> Each isotherm was fitted using a dual-site or single-site Langmuir–Freundlich model, with the chosen model based on the accuracy of the resulting fitting (Figures S17–S26). The selectivities for each mixture (Figures 3c and S27) are in agreement with the Henry's law calculations at 273 K, as the order of selectivity over  $\text{CH}_4$  is shown to be  $\text{C}_2\text{H}_4 > \text{C}_2\text{H}_2 \gg \text{C}_2\text{H}_6$ . At very low pressures ( $\sim 20$  mbar) the  $\text{C}_2\text{H}_4:\text{CH}_4$  selectivity is predicted to be 110:1, which decreases rapidly with increasing pressure before reaching 26:1 at 1 bar. The  $\text{C}_2\text{H}_2:\text{CH}_4$  selectivity is 97:1 below 30 mbar and decreases to 28:1 at 1 bar. At 298 K, the IAST predictions show that the selectivity for  $\text{C}_2\text{H}_4$  over  $\text{CH}_4$  is much greater than that of  $\text{C}_2\text{H}_2$  between 20 and 200 mbar (111:1 versus 51:1 at 20 mbar), although the selectivities are approximately equal at 1 bar.

The isosteric heats of adsorption ( $Q_{\text{st}}$ ) for each gas were calculated using a virial method to fit the sorption isotherms at 273 and 298 K. The heats of adsorption at zero loading for  $\text{CO}_2$ ,  $\text{C}_2\text{H}_2$ ,  $\text{C}_2\text{H}_4$ , and  $\text{C}_2\text{H}_6$  are 30, 37, 36, and 24  $\text{kJ mol}^{-1}$ , respectively. Each has a higher  $Q_{\text{st}}$  at zero loading than  $\text{CH}_4$  (23  $\text{kJ mol}^{-1}$ ). The values of  $Q_{\text{st}}$  follow the same pattern as the selectivities at 298 K ( $\text{C}_2\text{H}_2 > \text{C}_2\text{H}_4 \gg \text{C}_2\text{H}_6$ ), although at 273 K the  $\text{C}_2\text{H}_4:\text{CH}_4$  selectivity is greater than the  $\text{C}_2\text{H}_2:\text{CH}_4$  selectivity (130:1 versus 104:1).

**Solid-State  $^2\text{H}$  NMR Spectroscopic Studies of Activated and Gas-Loaded MFM-160.** In order to gain a greater understanding of the  $\text{C}_2\text{H}_2:\text{CO}_2$  separation and of the behavior of both gases within the porous material,  $^2\text{H}$  NMR spectroscopic studies were carried out on a partially deuterated analogue of MFM-160, denoted MFM-160-*d*<sub>12</sub> (Scheme 2). The dynamics of the phenyl ring can affect the adsorption properties in two ways: first, the phenyl rings themselves

### Scheme 2. Synthesis of $\text{H}_6\text{L-}d_{12}$



provide an accessible adsorption site as a result of the aromatic  $\pi$ -system; second, the phenyl rotation directly affects the effective size and geometry of the pore. Probing the framework dynamics is also of interest for comparison with other known MOFs, thus improving understanding of structure–property relationships. The rotational dynamics in MFM-160- $d_{12}$  were probed in the activated, desolvated material (Figures 4 and

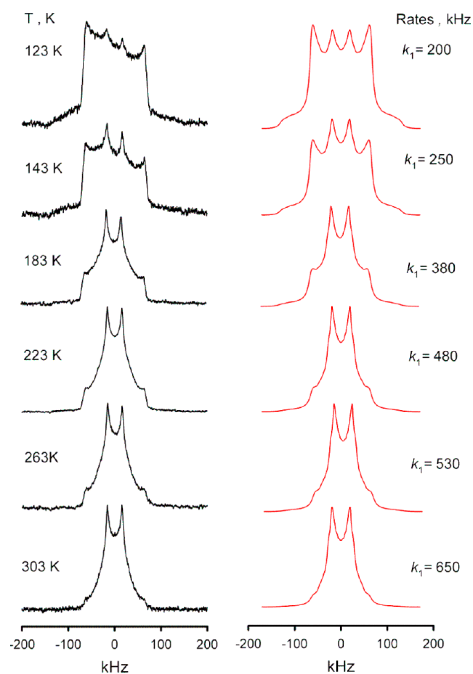


**Figure 4.** Temperature dependence of the line shape of resonances due to the phenyl groups in guest-free MFM-160- $d_{12}$  as measured by  $^2\text{H}$  NMR spectroscopy (experimental, black; simulation, red).

S28) in the presence of  $\text{CO}_2$  at 1 and 5 bar loadings (Figures S29 and S30, respectively) and in the presence of  $\text{C}_2\text{H}_2$  at 0.32 and 1 bar (Figures S31 and S32, respectively). As the low-

pressure uptake of  $\text{C}_2\text{H}_2$  is significantly higher than that of  $\text{CO}_2$ , respective pressures of 0.32 and 1 bar were chosen for comparison of the two gases at the same concentrations. The loadings of 0.32 bar of  $\text{C}_2\text{H}_2$  and 1 bar of  $\text{CO}_2$  each correspond to  $\sim 3.1$  gas molecules per linker, where the empirical formula of MFM-160- $d_{12}$  gives a density of  $1043.43 \text{ g mol}^{-1}$ . The higher loadings of 1 bar of  $\text{C}_2\text{H}_2$  and 5 bar of  $\text{CO}_2$  correspond to 5.9 and 10.8 molecules per linker, respectively.

In the activated, desolvated MFM-160- $d_{12}$ , the temperature-dependent behavior of the line shapes in the  $^2\text{H}$  NMR spectra confirms that the deuterated phenyl rings are mobile, with a dynamic process gradually developing between  $\sim 120$  and 300 K (Figures 4 and 5). Below 123 K the line shape is mainly composed of a Pake-powder pattern with quadrupolar coupling parameters ( $Q_0 = 176 \text{ kHz}$ ,  $\eta_0 \approx 0$ ) typical for a static C–D group on the  $^2\text{H}$  NMR spectroscopic time scale. At  $\sim 300 \text{ K}$ , the spectrum is dominated by the narrowed line shape expected for an axial rotation around the phenyl  $\text{C}_2$  axis ( $Q_1 \approx 20 \text{ kHz} \approx Q_0/8$ ).<sup>48</sup> At the same time, over the whole temperature range studied, these two components co-exist. Such a phenomenon has been reported for UiO-66<sup>49</sup> and indicates that the phenyl motion at each given temperature is characterized by a distribution of rotation rates, which suggests that the rotational potential fluctuates to a certain degree across the framework. In common with work by Schmidt et al.,<sup>50</sup> the rate constant is assumed to obey a log-normal distribution, with  $k_1$  being the mean value of the rotation rate at each given temperature and  $\sigma$  being the width of the distribution. By considering the  $\text{C}_2$  symmetry of the phenyl fragment, the uniaxial rotation around the  $\text{C}_2$  axis can be modeled by either a 4-site or a 6-site jump rotation model (Figure 6). Notably, in most cases the 6-site jump model can also efficiently describe more complex axial rotations.<sup>51</sup> Numerical fitting of the experimentally observed  $^2\text{H}$  NMR spectroscopic patterns shows that only the 6-site jump rotation gives an agreement with our data.

Although the distribution of the jump sites has to obey  $\text{C}_2$  symmetry, the initial position of the phenyl orientation might be distorted from a fully symmetric case. This distortion is

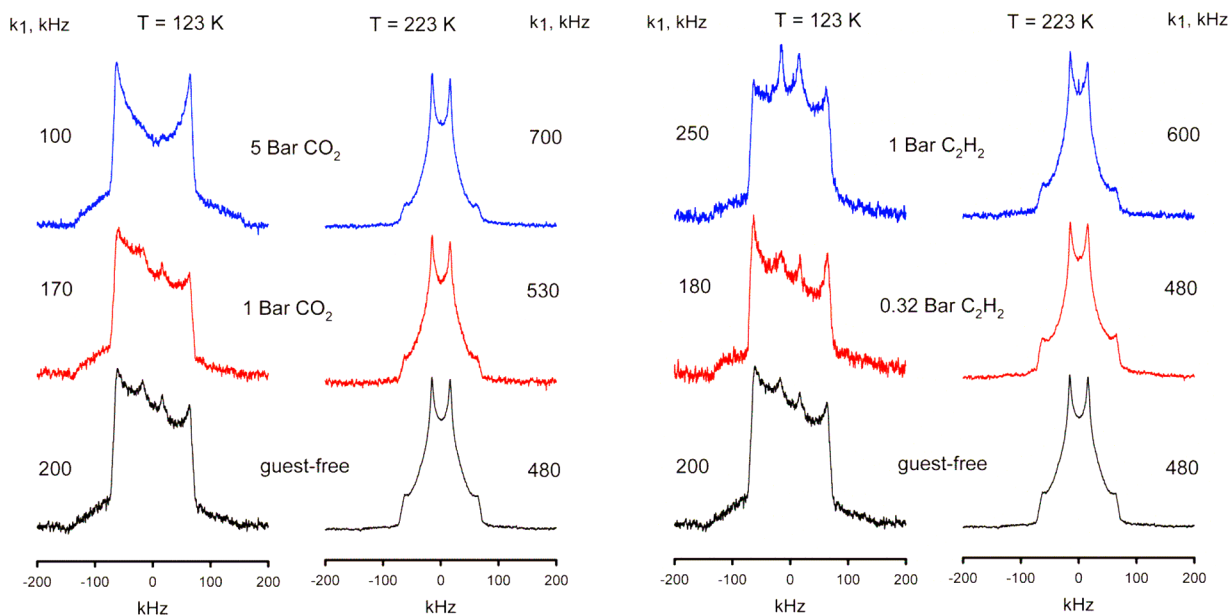


**Figure 5.** Comparison of the experimental line shapes and rotation rates for phenyl groups in guest-loaded MFM-160- $d_{12}$  at 123 and 223 K.

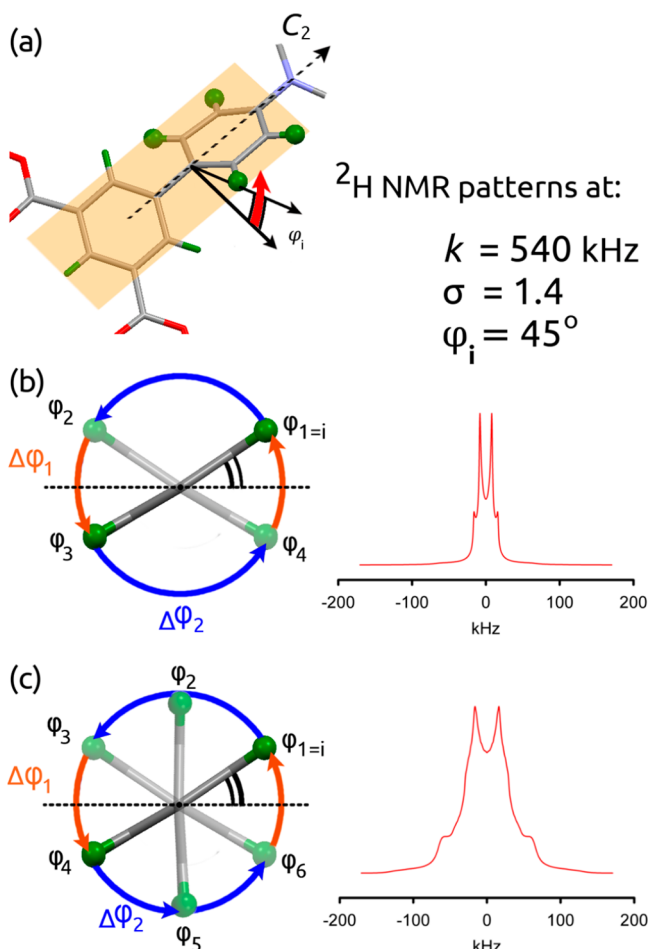


**Figure 6.** View of stable orientation sites for the phenyl rings depending on the jump rotation model. (a) The starting position of the mobile phenyl ring is tilted by an angle  $\varphi_i$ . The axial jump rotation about the  $C_2$  symmetry axis of the phenyl group is then realized by either (b) an  $n = 4$  site exchange motion or (c) an  $n = 6$  site exchange. The distribution of the orientation sites is governed only by the value of the first position,  $\varphi_1 = \varphi_i$ . All elementary jumps are assumed to be governed by the same rate constant,  $k = k_i/n$ . Even in the case of the same value of  $\varphi_i$  in the intermediate jump rate, the two models give qualitatively distinct patterns.

readily introduced into the re-orientation model as an angular parameter  $\varphi_i$  (Figure 6). For a 6-site jump rotation mechanism, the jump positions are given as follows:  $\varphi_1 = \varphi_i$ ,  $\varphi_2 = \pi/2$ ,  $\varphi_3 = \pi - \varphi_1$ ,  $\varphi_4 = \pi + \varphi_1$ ,  $\varphi_5 = \pi/2$ ,  $\varphi_6 = \pi + \varphi_2$ . Within such a model, we assume that all positions have equal probability. In our model, the angle  $\varphi_i = 45^\circ$ , where  $\varphi_i$  is the angle between the plane of the mobile phenyl ring and the plane of the aromatic ring fixed to the Cu(II) node. Thus, it follows that the value  $\Delta\varphi_1 = 2\varphi_i$  can be directly compared with the crystal structure. Despite the model being able to give distinct rate constants for each elementary jump, we have found that a simple kinetic matrix defined by one rate constant is sufficient to provide good agreement with the experimental observations. Thus, this 6-site jump rotation model accurately simulates the experimental temperature dependence of the  $^2\text{H}$  NMR spectral line shapes. The model  $\Delta\varphi_1 = 2\varphi_i \approx 90^\circ$  is consistent with the crystallographic data and underscores that the orientation of the phenyl rings is not homogeneously distributed. The log-normal distribution width is almost constant over the temperature range:  $\sigma \approx 1.3\text{--}1.4$ . Thus, the present

inhomogeneity is considerably lower than that observed in UiO-66 and may be attributed to the flexible nature of MFM-160.

The most striking features of the  $^2\text{H}$  NMR spectra for MFM-160- $d_{12}$  are the kinetic parameters of the deuterated phenyl motion. The Arrhenius plot (Figure 7a) is linear and

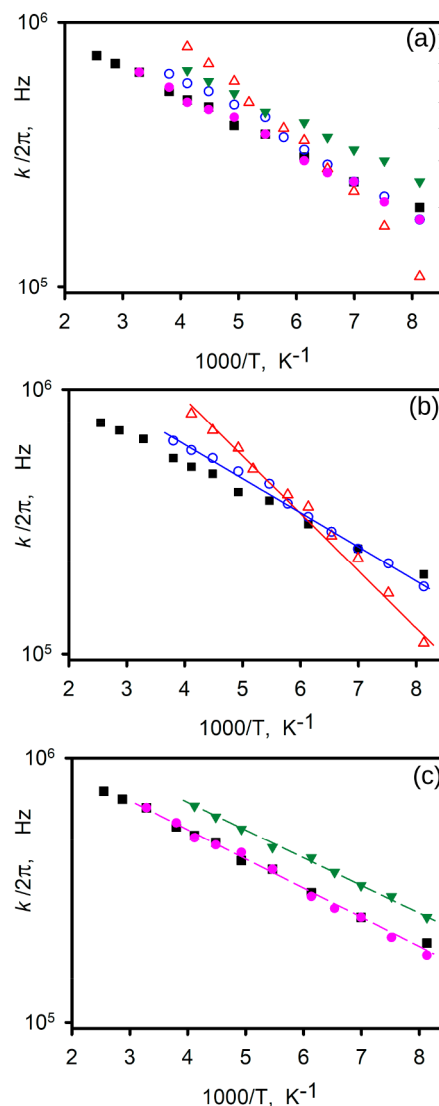


**Figure 7.** Arrhenius plots of the rotation rate constants  $k_1$ : (a) of all gas-loaded samples, (b) of  $\text{CO}_2$ -loaded MFM-160, and (c) of  $\text{C}_2\text{H}_2$ -loaded MFM-160. (■) Guest-free MFM-160- $d_{12}$ ; (blue ○) 1 bar  $\text{CO}_2$  loading; (red Δ) 5 bar  $\text{CO}_2$  loading; (pink ●) 0.32 bar  $\text{C}_2\text{H}_2$  loading; (dark green ▼) 1 bar  $\text{C}_2\text{H}_2$  loading. All gas loadings were performed at 298 K.

shows an activation barrier,  $E_0 = 2.1 \text{ kJ mol}^{-1}$ , and collision factor,  $k_{00}/2\pi = 1.4 \times 10^6 \text{ Hz}$ . This activation barrier is so low that it is comparable to the torsional barrier for methyl groups in xylenes or 2-methylimidazole, i.e., aromatic systems where the internal steric interactions are minimized. The torsional barrier for methyl groups in such compounds has been measured experimentally by neutron scattering techniques and  $^2\text{H}$  NMR spectroscopy, which confirm in both cases that  $E_0$  does not exceed  $1.5 \text{ kJ mol}^{-1}$ .<sup>52,53</sup> Such low values have not been reported previously for solid-state materials based upon carboxylate ligands but have been confirmed for many different

samples of MFM-160-*d*<sub>12</sub>. However, similar low barriers have been reported recently for MOFs incorporating metal–amine linkers, such as 2-methylimidazole in ZIF-8<sup>52</sup> and dabco in [Zn<sub>2</sub>(bdc)<sub>2</sub>(dabco)].<sup>54</sup>

It is interesting to consider the possible sources of steric interaction hindering phenyl rotation in MFM-160-*d*<sub>12</sub>. The electrostatic interactions are maximized when all aromatic rings are in the same plane, in which case the closest interatomic distances can be given as  $d_1 \approx 2.2$  Å,  $d_2 \approx 3.1$  Å, and  $d_3 \approx 2.0$  Å (Figure 8). The main interaction is likely governed by sites III

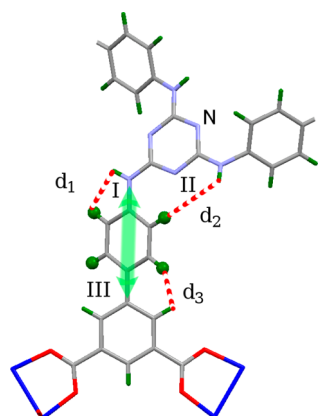


**Figure 8.** View of the deuterated (green) mobile phenyl ring in MFM-160-*d*<sub>12</sub>. The scheme shows the possible hydrogen-bonding sites (I, II, and III) that will influence the rotational potential for rotation of the phenyl group.

and I, but these distances do not offer an obvious explanation for the ultra-low value of  $k_{00}$  (usually  $\sim 10^{11-13}$  Hz in MOF materials). However, this may be explained by the short intramolecular hydrogen bond (1.91 Å) between the phenyl protons and the triazine N atoms observed in the crystal structure, thus restricting the rotation of the ring by affecting its pre-exponential factor.

Although the effect of gas loading is not very strong in terms of absolute values, it is an unexpected one (Figure 5). With CO<sub>2</sub> as the guest species, the concentration dependence at 123 K is as expected, with a higher gas loading resulting in a slower rate of phenyl rotation. At the higher loading of  $\sim 5$  bar (at 298 K), the decrease in rotation rate is also more evident, even without detailed numerical analysis of the observed line shape. However, at 223 K this effect is inverted: with increased loading of CO<sub>2</sub>, the rate of phenyl rotation actually increases, a phenomenon previously unobserved in a MOF or any other solid-state material.<sup>55</sup> On a quantitative level, the effect is clearly seen on an Arrhenius plot (Figure 7b) for the corresponding rotational rate constants: the slope for the CO<sub>2</sub>-loaded material is notably steeper in comparison to that of the guest-free material. While not very pronounced for the intermediate loading (1 bar), with  $E_1 = 2.6$  kJ mol<sup>-1</sup> and  $k_{10}/2\pi = 2.3 \times 10^6$  Hz, the effect becomes more evident at higher concentration (5 bar), with  $E_2 = 4.2$  kJ mol<sup>-1</sup> and  $k_{20}/2\pi = 7.6 \times 10^6$  Hz. In the latter case the barrier is approximately doubled compared with that of the desolvated material, but the collision factor is increased by 6-fold, so even though the barrier has increased, the collision factor overrides this, suggesting that CO<sub>2</sub> blocks or breaks the internal H-bonding, thus allowing more rapid rotation of the phenyl groups. It is possible to readily observe the collision factor behavior because

of the extremely low starting value for the guest-free material, i.e.,  $k_{00}/2\pi = 1.4 \times 10^6$  Hz, while normal pre-exponential factors for an elementary rotation are typically in the range of  $10^{11-13}$  Hz.

For the C<sub>2</sub>H<sub>2</sub>-loaded material, the situation is different: at the intermediate concentration ( $\sim 0.32$  bar at room temperature), conditions in which the C<sub>2</sub>H<sub>2</sub> concentration is equimolar to that of CO<sub>2</sub> at 1 bar, no effect on the phenyl dynamics is observed (Figure 7c), and the rotation is characterized by the same parameters as for the activated, desolvated MFM-160-*d*<sub>12</sub>, with  $E_3 = 1.9$  kJ mol<sup>-1</sup> and  $k_{30} = 1.2 \times 10^6$  Hz. Upon increasing the C<sub>2</sub>H<sub>2</sub> concentration to 1 bar, the rate of phenyl ring rotation clearly increases; however, the activation barrier remains the same,  $E_4 = 1.9$  kJ mol<sup>-1</sup>, but the collision factor rises to  $k_{40} = 1.8 \times 10^6$  Hz. This is shown on the corresponding Arrhenius plots (Figure 7c).

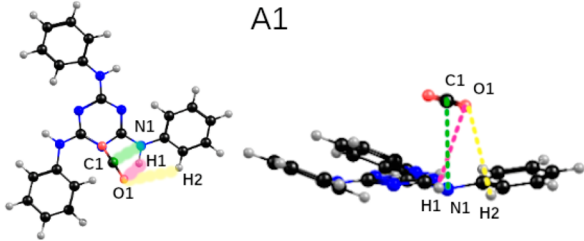
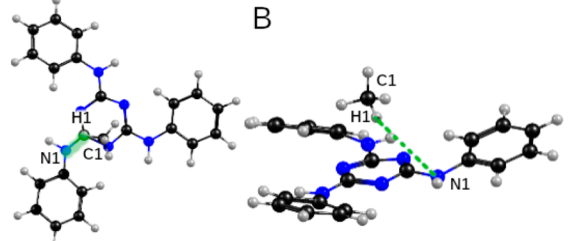
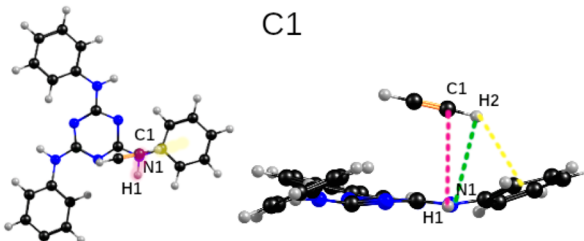
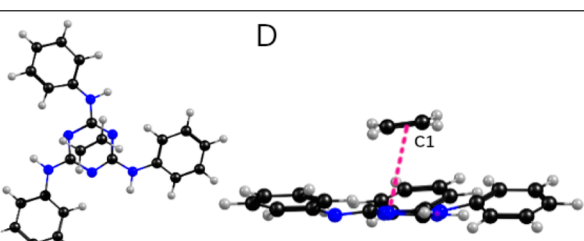
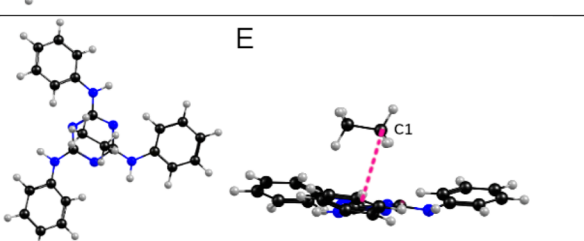
This behavior can be interpreted in terms of host–guest interactions. At the lower loading the phenyl rings do not interact with C<sub>2</sub>H<sub>2</sub>, and only at higher loadings is there a subtle increase of the collision factor. This shows that the occupancy of C<sub>2</sub>H<sub>2</sub> sites around the mobile phenyl rings is low, even at higher concentrations. Thus, C<sub>2</sub>H<sub>2</sub> coordinates predominantly to the Cu(II) paddlewheel sites and interacts with the phenyl rings only through random collisions, most likely when most of the metal sites are occupied. At 0.32 bar of C<sub>2</sub>H<sub>2</sub> (3.1 gas molecules per formula unit), the Cu(II) sites are very likely saturated, with C<sub>2</sub>H<sub>2</sub> bound strongly and not able to influence phenyl rotation, as shown by <sup>2</sup>H NMR spectroscopy.

However, with an equimolar loading of CO<sub>2</sub>, where the Cu(II) sites were also expected to be saturated, the phenyl ring rotation is much more affected by the guest CO<sub>2</sub> molecules than for C<sub>2</sub>H<sub>2</sub>, strongly suggesting that CO<sub>2</sub> occupies binding sites on the linker, while open Cu(II) sites are still available. These observations, therefore, provide a good insight into the selectivity for C<sub>2</sub>H<sub>2</sub> over CO<sub>2</sub>, as the stronger binding of C<sub>2</sub>H<sub>2</sub> at the open Cu(II) sites very likely accounts for the greater uptake of C<sub>2</sub>H<sub>2</sub> at low pressures. Interestingly, the C<sub>2</sub>H<sub>2</sub>:CO<sub>2</sub> selectivity in [Cu<sub>2</sub>(pzdc)<sub>2</sub>(pyz)] (pzdc<sup>2-</sup> = pyrazine-2,3-dicarboxylate; pyz = pyrazine), a MOF without open Cu(II) sites, was assigned to the binding of C<sub>2</sub>H<sub>2</sub> with free carboxylate oxygen atoms lining the pores.<sup>56</sup>

**Computational Modeling of Gas Binding Sites in MFM-160.** To understand further the observations from <sup>2</sup>H NMR spectroscopy and to help explain the hydrocarbon selectivity demonstrated by MFM-160a, DFT calculations were performed using the Q-Chem quantum chemistry package.<sup>36</sup>

An extensive search for binding sites between all guest molecules and the linker fragment was performed, with configurations showing the strongest binding and binding energy ranges summarized in Table 1; Table S2 shows the full range of binding configurations. The strongest binding of CO<sub>2</sub> to the linker fragment was found to be at site A1 (Table 1), in which the CO<sub>2</sub> molecule interacts above the linker, with a binding energy of  $-19.5$  kJ mol<sup>-1</sup>. The interaction is dominated by a strong electrostatic interaction between the carbon of CO<sub>2</sub> and the N-center of the central ring. This interaction is enhanced by two weak hydrogen bonds between the other oxygen of CO<sub>2</sub> and nearby protons of the neighboring phenyl ring and the bridging –NH group. These interactions have a significant cooperative effect on the binding of CO<sub>2</sub> to the linker fragment. The slow rotation of the phenyl ring, as observed by <sup>2</sup>H NMR spectroscopy, was attributed to a hydrogen bond between a phenyl proton and a

**Table 1.** Optimized B3LYP/B3LYP/6-31+G\* and B3LYP/6-311+G\* Binding Energies and Structural Details of C<sub>21</sub>H<sub>18</sub>N<sub>6</sub>–Guest Molecule Complexes Corresponding to These Strongest Binding Energies

Guests	Optimised geometry	Parameters
CO <sub>2</sub>	 <p style="text-align: center;">A1</p>	Binding energy: $\Delta E = -19.5 \text{ kJ mol}^{-1}$ Distance C–N1...C1 (CO <sub>2</sub> ): 3.25 Å Distance N–H1...O1 (CO <sub>2</sub> ): 3.00 Å Distance C–H2...O1 (CO <sub>2</sub> ): 2.98 Å Angle C–N1...C1 (CO <sub>2</sub> ): 104.63° Angle N1–H1...O1 (CO <sub>2</sub> ): 103.39° Angle C–H2...O1 (CO <sub>2</sub> ): 129.12°
CH <sub>4</sub>	 <p style="text-align: center;">B</p>	Binding energy: $\Delta E = -10.3 \text{ kJ mol}^{-1}$ Distance C–N1...H1 (CH <sub>4</sub> ): 2.97 Å Distance (C <sub>3</sub> N <sub>3</sub> )...H (CH <sub>4</sub> ): 3.32 Å Angle C–N1...H1 (CH <sub>4</sub> ): 93.79° Angle ring...C1 (CH <sub>4</sub> ): 100.02°
C <sub>2</sub> H <sub>2</sub>	 <p style="text-align: center;">C1</p>	Binding energy: $\Delta E = -18.2 \text{ kJ mol}^{-1}$ Distance H–N1...C1 (C <sub>2</sub> H <sub>2</sub> ): 3.35 Å Distance C–N1...H2 (C <sub>2</sub> H <sub>2</sub> ): 3.70 Å Distance (C <sub>6</sub> H <sub>5</sub> )...H2 (C <sub>2</sub> H <sub>2</sub> ): 2.28 Å Angle H–N1...C1 (C <sub>2</sub> H <sub>2</sub> ): 98.80° Angle C–N1...H2 (C <sub>2</sub> H <sub>2</sub> ): 93.05° Angle (C <sub>6</sub> H <sub>5</sub> )...H2 (C <sub>2</sub> H <sub>2</sub> ): 108.73°
C <sub>2</sub> H <sub>4</sub>	 <p style="text-align: center;">D</p>	Binding energy: $\Delta E = -16.2 \text{ kJ mol}^{-1}$ Distance (C <sub>3</sub> N <sub>3</sub> )...(C <sub>2</sub> H <sub>4</sub> ): 3.33 Å Angle (C <sub>3</sub> N <sub>3</sub> )...C1 (C <sub>2</sub> H <sub>4</sub> ): 78.47°
C <sub>2</sub> H <sub>6</sub>	 <p style="text-align: center;">E</p>	Binding energy: $\Delta E = -16.3 \text{ kJ mol}^{-1}$ Distance (C <sub>3</sub> N <sub>3</sub> )...(C <sub>2</sub> H <sub>6</sub> ): 3.55 Å Angle (C <sub>3</sub> N <sub>3</sub> )...C1 (C <sub>2</sub> H <sub>6</sub> ): 75.95°

N atom of the triazine core. Therefore, the increased rotation upon CO<sub>2</sub> loading may be explained by the weakening or removal of this hydrogen bond upon CO<sub>2</sub> binding at site A1. Increased occupancy at this site at higher CO<sub>2</sub> loading would also explain the increased rate of rotation from the 1 bar- to the 5 bar-loaded sample. Overall, CO<sub>2</sub> interacts more strongly with the linker fragment than C<sub>2</sub>H<sub>2</sub>, giving a range of binding energies from  $-19.5$  to  $-12.4 \text{ kJ mol}^{-1}$ .

The strongest binding site for C<sub>2</sub>H<sub>2</sub> is over the bridging amine nitrogen between the triazine ring and the outer phenyl rings, with a binding energy of  $-18.2 \text{ kJ mol}^{-1}$  (site C1, Table 1). There is a cooperative binding effect, with the hydrogens of

C<sub>2</sub>H<sub>2</sub> interacting with the triazine ring and the neighboring phenyl ring, but the binding is dominated by an interaction between the  $\pi$ -bonds of the C<sub>2</sub>H<sub>2</sub> and the bridging nitrogen. As with CO<sub>2</sub>, this interaction is likely to affect the hydrogen bond between the phenyl proton and the triazine core, leading to the increased phenyl rotation rate observed by <sup>2</sup>H NMR spectroscopy upon addition of 1 bar C<sub>2</sub>H<sub>2</sub>. At lower pressures (0–0.32 bar), this site is unoccupied, as confirmed by the values of  $E_0$  and  $k_{00}$  at 0.32 bar remaining the same as those observed in the guest-free material. Between 0.32 and 1 bar, where the Cu(II) paddlewheel sites are expected to be saturated, the increased occupancy of this site disrupts the

intramolecular hydrogen bond of the linker, and the rotation of the phenyl group increases. It would have been interesting to observe the effect of a higher loading of  $C_2H_2$  on the rotational dynamics, but there are well-established safety concerns with the use of  $C_2H_2$  above 1 bar.

The  $\pi$ -bond interaction of  $C_2H_2$  with the linker leads to stronger interactions overall compared to other hydrocarbons, and as a result the  $C_2H_2$  molecule interacts with a similar range of binding energies to  $O_2$  ( $-13.3$  to  $-18.2$   $\text{kJ mol}^{-1}$ ). These comparable binding energies strongly suggest that the triazine functionality is not responsible for the selectivity for  $C_2H_2$  over  $CO_2$ . As stated earlier, it is likely that increased van der Waals interactions between  $C_2H_2$  and the framework in comparison to those with  $CO_2$ , as well as the higher affinity of the former for the open Cu(II) sites, are responsible for the selective uptake.

The ranges of interactions between the hydrocarbons  $C_2H_4$  and  $C_2H_6$  and the linker were also investigated and found to be very similar:  $-11.7$  to  $-16.2$   $\text{kJ mol}^{-1}$  and  $-10.2$  to  $-16.3$   $\text{kJ mol}^{-1}$ , respectively. The strongest interaction, between  $C_2H_4$  and the linker and also  $C_2H_6$  and the linker, occurs over the central triazine ring. This is an interaction between the central carbon–carbon bond of the two hydrocarbons,  $C_2H_4$  and  $C_2H_6$ , and the delocalized  $\pi$ -system of the central ring. On average, the binding of  $C_2H_4$  is stronger than that of  $C_2H_6$  due to the strength of the interaction between the alkene double bond and the linker.

To complete the computational investigation, we found that the strongest binding of  $CH_4$  to the linker was in complex B (Table 1), where the  $CH_4$  molecule interacts above the central triazine ring to give a binding energy of  $-10.3$   $\text{kJ mol}^{-1}$ . There is a weak hydrogen bond between a  $CH_4$  hydrogen atom and a nitrogen atom of the triazine ring. There are also additional weak electrostatic interactions between other  $CH_4$  hydrogen atoms and the central ring. The binding energy interactions between  $CH_4$  and the linker are the weakest of all those studied, consistent with the experimental isotherm data.

## CONCLUSIONS

We have demonstrated an energy- and cost-efficient route to a large hexacarboxylate linker through microwave-assisted synthesis. This has led to the synthesis of a new, highly porous (3,24)-connected Cu(II) MOF, designated MFM-160. We have shown that its activated form, MFM-160a, exhibits an exceptional capacity for uptake of  $CO_2$  at 20 bar and 298 K (110 wt%). We have also shown that the relatively poor uptake of  $CO_2$  and  $CH_4$  at lower pressures ( $\leq 1$  bar) makes MFM-160a a material of interest for the purification of natural gas and of acetylene, as confirmed by Henry's law and IAST calculations. A  $^2H$  NMR spectroscopic study of phenyl rotation dynamics confirmed an ultra-low rotation barrier but very slow phenyl rotation. The rotation was shown to increase upon gas loading, a unique phenomenon not previously observed in a solid-state material, which is attributed to the weakening of an intramolecular hydrogen bond upon gas binding, leading to an increased rate of rotation. The results of DFT calculations are consistent with this, as both gases show clear binding interactions near this hydrogen bond.

## ASSOCIATED CONTENT

### Supporting Information

The Supporting Information is available free of charge at <https://pubs.acs.org/doi/10.1021/jacs.0c11202>.

Experimental details, Scheme S1, Figures S1–S33, and Tables S1–S3 (PDF)

## Accession Codes

CCDC 1522524 contains the supplementary crystallographic data for this paper. These data can be obtained free of charge via [www.ccdc.cam.ac.uk/data\\_request/cif](http://www.ccdc.cam.ac.uk/data_request/cif), or by emailing [data\\_request@ccdc.cam.ac.uk](mailto:data_request@ccdc.cam.ac.uk), or by contacting The Cambridge Crystallographic Data Centre, 12 Union Road, Cambridge CB2 1EZ, UK; fax: +44 1223 336033.

## AUTHOR INFORMATION

### Corresponding Authors

**Sihai Yang** – School of Chemistry, University of Manchester, Manchester M13 9PL, U.K.; [orcid.org/0000-0002-1111-9272](https://orcid.org/0000-0002-1111-9272); Email: [sihai.yang@nottingham.ac.uk](mailto:sihai.yang@nottingham.ac.uk)

**Martin Schröder** – School of Chemistry, University of Manchester, Manchester M13 9PL, U.K.; [orcid.org/0000-0001-6992-0700](https://orcid.org/0000-0001-6992-0700); Email: [m.schroder@nottingham.ac.uk](mailto:m.schroder@nottingham.ac.uk)

**Daniil I. Kolokolov** – Boreskov Institute of Catalysis, Siberian Branch of Russian Academy of Sciences, Novosibirsk 630090, Russia; Novosibirsk State University, Novosibirsk 630090, Russia; Email: [daniil.kolokolov@gmail.com](mailto:daniil.kolokolov@gmail.com)

**Timothy L. Easun** – School of Chemistry, University of Nottingham, Nottingham NG7 2RD, U.K.; School of Chemistry, Cardiff University, Cardiff CF10 3AT, U.K.; [orcid.org/0000-0002-0713-2642](https://orcid.org/0000-0002-0713-2642); Email: [EasunTL@cardiff.ac.uk](mailto:EasunTL@cardiff.ac.uk)

### Authors

**William J. F. Trenholme** – School of Chemistry, University of Manchester, Manchester M13 9PL, U.K.; School of Chemistry, University of Nottingham, Nottingham NG7 2RD, U.K.

**Michelle Bound** – School of Chemistry, University of Nottingham, Nottingham NG7 2RD, U.K.

**Stephen P. Argent** – School of Chemistry, University of Nottingham, Nottingham NG7 2RD, U.K.

**Jamie A. Gould** – School of Chemistry, University of Nottingham, Nottingham NG7 2RD, U.K.; Faculty of Science, Agriculture and Engineering, Newcastle University, Newcastle upon Tyne NE1 7RU, U.K.

**Jiangnan Li** – School of Chemistry, University of Manchester, Manchester M13 9PL, U.K.

**Sarah A. Barnett** – Diamond Light Source, Harwell Science and Innovation Campus, Didcot, Oxfordshire OX11 0DE, U.K.

**Alexander J. Blake** – School of Chemistry, University of Nottingham, Nottingham NG7 2RD, U.K.

**Alexander G. Stepanov** – Boreskov Institute of Catalysis, Siberian Branch of Russian Academy of Sciences, Novosibirsk 630090, Russia; Novosibirsk State University, Novosibirsk 630090, Russia; [orcid.org/0000-0003-2754-5273](https://orcid.org/0000-0003-2754-5273)

**Elena Besley** – School of Chemistry, University of Nottingham, Nottingham NG7 2RD, U.K.; [orcid.org/0000-0002-9910-7603](https://orcid.org/0000-0002-9910-7603)

Complete contact information is available at: <https://pubs.acs.org/doi/10.1021/jacs.0c11202>

### Notes

The authors declare no competing financial interest.

## ACKNOWLEDGMENTS

We thank the EPSRC, the University of Nottingham, and the University of Manchester for funding. This project has received funding to M.S. from the European Research Council (ERC) under the European Union's Horizon 2020 research and innovation programme (grant agreement no. 742401, NANO-CHEM). We are very grateful to Diamond Light Source for access to Beamline I19. W.J.F.T. thanks Johnson Matthey for funding and Dr. Hugh Hamilton and Dr. Ian Casely for valuable discussions. T.L.E. gratefully acknowledges the Royal Society for the award of a University Research Fellowship. M.S. and D.I.K. gratefully acknowledge receipt of the Royal Society International Exchanges Scheme grant ref IE150114. D.I.K. also acknowledges the support from the Russian Science Foundation, project 17-73-10135. D.I.K. and A.G.S. also acknowledge the support of Ministry of Science and High Education of the Russian Federation (project AAAA-A21-121011390053-4, Boreskov Institute of Catalysis). E.B. and M.B. acknowledge the High Performance Computing (HPC) Facility at the University of Nottingham for providing computational time. J.L. also thanks the China Scholarship Council (CSC) for funding.

## REFERENCES

- (1) Chen, K. J.; Scott, H. S.; Madden, D. G.; Pham, T.; Kumar, A.; Bajpai, A.; Lusi, M.; Forrest, K. A.; Space, B.; Perry, J. J.; Zaworotko, M. J. Benchmark  $C_2H_2/CO_2$  and  $CO_2/C_2H_2$  separation by two closely related hybrid ultramicroporous materials. *Chem* **2016**, *1*, 753–765.
- (2) Ding, M.; Flaig, R. W.; Jiang, H. L.; Yaghi, O. M. Carbon capture and conversion using metal–organic frameworks and MOF-based materials. *Chem. Soc. Rev.* **2019**, *48*, 2783–2828.
- (3) Alsmail, N. H.; Suyetin, M.; Yan, Y.; Cabot, R.; Krap, C. P.; Lü, J.; Easun, T. L.; Bichoutskaia, E.; Lewis, W.; Blake, A. J.; Schröder, M. Analysis of high and selective uptake of  $CO_2$  in an oxamide-containing  $\{Cu_2(OOCR)_4\}$ -based metal–organic framework. *Chem. - Eur. J.* **2014**, *20*, 7317–7324.
- (4) An, J.; Geib, S. J.; Rosi, N. L. High and selective  $CO_2$  uptake in a cobalt adeninate metal–organic framework exhibiting pyrimidine- and amino-decorated pores. *J. Am. Chem. Soc.* **2010**, *132*, 38–39.
- (5) Millward, A. R.; Yaghi, O. M. Metal–organic frameworks with exceptionally high capacity for storage of carbon dioxide at room temperature. *J. Am. Chem. Soc.* **2005**, *127*, 17998–17999.
- (6) Forse, A. C.; Milner, P. J.; Lee, J. H.; Redfean, H. N.; Oktawiec, J.; Siegelman, R. L.; Martell, J. D.; Dinakar, B.; Porter-Zasada, L. B.; Gonzalez, M. I.; Neaton, J. B.; Long, J. R.; Reimer, J. A. Elucidating  $CO_2$  chemisorption in diamine-appended metal–organic frameworks. *J. Am. Chem. Soc.* **2018**, *140*, 18016–18031.
- (7) Yang, S.; Sun, J.; Ramirez-Cuesta, A. J.; Callear, S. K.; David, W. I. F.; Anderson, D. P.; Newby, R.; Blake, A. J.; Parker, J. E.; Tang, C. C.; Schröder, M. Selectivity and direct visualization of carbon dioxide and sulfur dioxide in a decorated porous host. *Nat. Chem.* **2012**, *4*, 887–894.
- (8) Carrington, E. J.; McAnally, C. A.; Fletcher, A. J.; Thompson, S. P.; Warren, M.; Brammer, L. Solvent-switchable continuous-breathing behaviour in a diamondoid metal–organic framework and its influence on  $CO_2$  versus  $CH_4$  selectivity. *Nat. Chem.* **2017**, *9*, 882–889.
- (9) Yang, L.; Qian, S.; Wang, X.; Cui, X.; Chen, B.; Xing, H. Energy-efficient separation alternatives: metal–organic frameworks and membranes for hydrocarbon separation. *Chem. Soc. Rev.* **2020**, *49*, 5359–5406.
- (10) Hu, F.; Di, Z.; Wu, M.; Li, J. Building a robust 3D Ca-MOF by a new square  $Ca_4O$  SBU for purification of natural gas. *Dalt. Trans.* **2020**, *49*, 8836–8840.
- (11) Liu, K.; Ma, D.; Li, B.; Li, Y.; Yao, K.; Zhang, Z.; Han, Y.; Shi, Z. High storage capacity and separation selectivity for  $C_2$  hydrocarbons over methane in the metal–organic framework Cu–TDPAT. *J. Mater. Chem. A* **2014**, *2*, 15823–15828.
- (12) Li, Q.; Wu, N.; Li, J.; Wu, D.; Li, Y. Amino-functionalized water-stable metal–organic framework for enhanced  $C_2H_2/CH_4$  separation performance. *Inorg. Chem.* **2020**, *59*, 2631–2635.
- (13) Xu, H.; Cai, J.; Xiang, S.; Zhang, Z.; Wu, C.; Rao, X.; Cui, Y.; Yang, Y.; Krishna, R.; Chen, B.; Qian, G. A cationic microporous metal–organic framework for highly selective separation of small hydrocarbons at room temperature. *J. Mater. Chem. A* **2013**, *1*, 9916–9921.
- (14) He, Y.; Song, C.; Ling, Y.; Wu, C.; Krishna, R.; Chen, B. A new MOF-5 homologue for selective separation of methane from  $C_2$  hydrocarbons at room temperature. *APL Mater.* **2014**, *2*, 124102–124106.
- (15) Barnett, B. R.; Gonzalez, M. I.; Long, J. R. Recent progress towards light hydrocarbon separations using metal–organic frameworks. *Trends Chem.* **2019**, *1*, 159–171.
- (16) Rackley, S. A. *Carbon capture and storage*; Butterworth-Heinemann, 2010.
- (17) Li, J.-R.; Ma, Y.; McCarthy, M. C.; Sculley, J.; Yu, J.; Jeong, H.-K.; Balbuena, P. B.; Zhou, H.-C. Carbon dioxide capture-related gas adsorption and separation in metal–organic frameworks. *Coord. Chem. Rev.* **2011**, *255*, 1791–1823.
- (18) Zheng, B.; Bai, J.; Duan, J.; Wojtas, L.; Zaworotko, M. J. Enhanced  $CO_2$  binding affinity of a high-uptake rht-type metal–organic framework decorated with acylamide groups. *J. Am. Chem. Soc.* **2011**, *133*, 748–751.
- (19) Yuan, D.; Zhao, D.; Sun, D.; Zhou, H.-C. An isoreticular series of metal–organic frameworks with dendritic hexacarboxylate ligands and exceptionally high gas-uptake capacity. *Angew. Chem., Int. Ed.* **2010**, *49*, 5357–5361.
- (20) Furukawa, H.; Ko, N.; Go, Y. B.; Aratani, N.; Choi, S. B.; Choi, E.; Yazaydin, A. O.; Snurr, R. Q.; O'Keeffe, M.; Kim, J.; Yaghi, O. M. Ultrahigh porosity in metal–organic frameworks. *Science* **2010**, *329*, 424–428.
- (21) Llewellyn, P. L.; Bourrelly, S.; Serre, C.; Vimont, A.; Daturi, M.; Hamon, L.; De Weireld, G.; Chang, J.-S.; Hong, D.-Y.; Kyu Hwang, Y.; Hwa Jhung, S.; Férey, G. High uptakes of  $CO_2$  and  $CH_4$  in mesoporous metal–organic frameworks MIL-100 and MIL-101. *Langmuir* **2008**, *24*, 7245–7250.
- (22) Czaja, A. U.; Trukhan, N.; Müller, U. Industrial applications of metal–organic frameworks. *Chem. Soc. Rev.* **2009**, *38*, 1284–1293.
- (23) Liu, K.; Li, B.; Li, Y.; Li, X.; Yang, F.; Zeng, G.; Peng, Y.; Zhang, Z.; Li, G.; Shi, Z.; Feng, S.; Song, D. An N-rich metal–organic framework with an rht topology: high  $CO_2$  and  $C_2$  hydrocarbons uptake and selective capture from  $CH_4$ . *Chem. Commun.* **2014**, *50*, 5031–5033.
- (24) Yang, S.; Ramirez-Cuesta, A. J.; Newby, R.; Garcia-Sakai, V.; Manuel, P.; Callear, S. K.; Campbell, S. I.; Tang, C. C.; Schröder, M. Supramolecular binding and separation of hydrocarbons within a functionalized porous metal–organic framework. *Nat. Chem.* **2015**, *7*, 121–129.
- (25) Li, B.; Zhang, Z.; Li, Y.; Yao, K.; Zhu, Y.; Deng, Z.; Yang, F.; Zhou, X.; Li, G.; Wu, H.; Nijem, N.; Chabal, Y. J.; Lai, Z.; Han, Y.; Shi, Z.; Feng, S.; Li, J. Enhanced binding affinity, remarkable selectivity, and high capacity of  $CO_2$  by dual functionalization of a rht-type metal–organic framework. *Angew. Chem., Int. Ed.* **2012**, *51*, 1412–1415.
- (26) Luebke, R.; Eubank, J. F.; Cairns, A. J.; Belmabkhout, Y.; Wojtas, L.; Eddaoudi, M. The unique rht-mof platform, ideal for pinpointing the functionalization and  $CO_2$  adsorption relationship. *Chem. Commun.* **2012**, *48*, 1455–1457.
- (27) Yan, Y.; Lin, X.; Yang, S.; Blake, A. J.; Dailly, A.; Champness, N. R.; Hubberstey, P.; Schröder, M. Exceptionally high  $H_2$  storage by a metal–organic polyhedral framework. *Chem. Commun.* **2009**, 1025–1027.

- (28) Yan, Y.; Telepeni, I.; Yang, S.; Lin, X.; Kockelmann, W.; Dailly, A.; Blake, A. J.; Lewis, W.; Walker, G. S.; Allan, D. R.; Barnett, S. A.; Champness, N. R.; Schröder, M. Metal-organic polyhedral frameworks: high H<sub>2</sub> adsorption capacities and neutron powder diffraction studies. *J. Am. Chem. Soc.* **2010**, *132*, 4092–4094.
- (29) Yan, Y.; Blake, A. J.; Lewis, W.; Barnett, S. A.; Dailly, A.; Champness, N. R.; Schröder, M. Modifying cage structures in metal-organic polyhedral frameworks for H<sub>2</sub> storage. *Chem. - Eur. J.* **2011**, *17*, 11162–11170.
- (30) Yan, Y.; Yang, S.; Blake, A. J.; Lewis, W.; Poirier, E.; Barnett, S. A.; Champness, N. R.; Schröder, M. A mesoporous metal-organic framework constructed from a nanosized C<sub>3</sub>-symmetric linker and [Cu<sub>24</sub>(isophthalate)<sub>24</sub>] cuboctahedra. *Chem. Commun.* **2011**, *47*, 9995–9997.
- (31) Yan, Y.; Suyetin, M.; Bichoutskaia, E.; Blake, A. J.; Allan, D. R.; Barnett, S. A.; Schröder, M. Modulating the packing of [Cu<sub>24</sub>(isophthalate)<sub>24</sub>] cuboctahedra in a triazole-containing metal-organic polyhedral framework. *Chem. Sci.* **2013**, *4*, 1731–1736.
- (32) Yan, Y.; Yang, S.; Blake, A. J.; Schröder, M. Studies on metal-organic frameworks of Cu(II) with isophthalate linkers for hydrogen storage. *Acc. Chem. Res.* **2014**, *47*, 296–307.
- (33) Farha, O. K.; Özgür Yazaydın, A.; Eryazici, I.; Malliakas, C. D.; Hauser, B. G.; Kanatzidis, M. G.; Nguyen, S. T.; Snurr, R. Q.; Hupp, J. T. De novo synthesis of a metal-organic framework material featuring ultrahigh surface area and gas storage capacities. *Nat. Chem.* **2010**, *2*, 944–948.
- (34) Farha, O. K.; Eryazici, I.; Jeong, N. C.; Hauser, B. G.; Wilmer, C. E.; Sarjeant, A. A.; Snurr, R. Q.; Nguyen, S. T.; Yazaydın, A. Ö.; Hupp, J. T. Metal-organic framework materials with ultrahigh surface areas: is the sky the limit? *J. Am. Chem. Soc.* **2012**, *134*, 15016–15021.
- (35) Farha, O. K.; Wilmer, C. E.; Eryazici, I.; Hauser, B. G.; Parilla, P. A.; O'Neill, K.; Sarjeant, A. A.; Nguyen, S. T.; Snurr, R. Q.; Hupp, J. T. Designing higher surface area metal-organic frameworks: are triple bonds better than phenyls? *J. Am. Chem. Soc.* **2012**, *134*, 9860–9863.
- (36) Shao, Y.; Molnar, L. F.; Jung, Y.; Kussmann, J.; Ochsenfeld, C.; Brown, S. T.; Gilbert, A. T. B.; Slipchenko, L. V.; Levchenko, S. V.; O'Neill, D. P.; DiStasio, R. A., Jr; Lochan, R. C.; Wang, T.; Beran, G. J. O.; Besley, N. A.; Herbert, J. M.; Yeh, Lin, C.; Van Voorhis, T.; Hung Chien, S.; Sodt, A.; Steele, R. P.; Rassolov, V. A.; Maslen, P. E.; Korambath, P. P.; Adamson, R. D.; Austin, B.; Baker, J.; Byrd, E. F. C.; Dachsel, H.; Doerksen, R. J.; Dreuw, A.; Dunietz, B. D.; Dutoi, A. D.; Furlani, T. R.; Gwaltney, S. R.; Heyden, A.; Hirata, S.; Hsu, C.-P.; Kedziora, G.; Khalliulin, R. Z.; Klunzinger, P.; Lee, A. M.; Lee, M. S.; Liang, W.; Lotan, I.; Nair, N.; Peters, B.; Proynov, E. I.; Pieniazek, P. A.; Min Rhee, Y.; Ritchie, J.; Rosta, E.; David Sherrill, C.; Simmonett, A. C.; Subotnik, J. E.; Woodcock, L. H., III; Zhang, W.; Bell, A. T.; Chakraborty, A. K.; Chipman, D. M.; Keil, F. J.; Warshel, A.; Hehre, W. J.; Schaefer, H. F., III; Kong, J.; Krylov, A. I.; Gill, P. M. W.; Head-Gordon, M. Advances in methods and algorithms in a modern quantum chemistry program package. *Phys. Chem. Chem. Phys.* **2006**, *8*, 3172–3191.
- (37) Sha, Y.; Dong, Y. Microwave assisted synthesis of 2,4,6-triaryl-amino-1,3,5-triazines as potential UV absorbent. *Synth. Commun.* **2003**, *33*, 2599–2604.
- (38) Spek, A. L. PLATON SQUEEZE: A tool for the calculation of the disordered solvent contribution to the calculated structure factors. *Acta Crystallogr., Sect. C: Struct. Chem.* **2015**, *71*, 9–18.
- (39) Peng, Y. L.; Pham, T.; Li, P.; Wang, T.; Chen, Y.; Chen, K. J.; Forrest, K. A.; Space, B.; Cheng, P.; Zaworotko, M. J.; Zhang, Z. Robust ultramicroporous metal-organic frameworks with benchmark affinity for acetylene. *Angew. Chem., Int. Ed.* **2018**, *57*, 10971–10975.
- (40) Pei, J.; Shao, K.; Wang, J. X.; Wen, H. M.; Yang, Y.; Cui, Y.; Krishna, R.; Li, B.; Qian, G. A chemically stable Hofmann-type metal-organic framework with sandwich-like binding sites for benchmark acetylene capture. *Adv. Mater.* **2020**, *32*, 1908275.
- (41) Chen, Z.; Xiang, S.; Arman, H. D.; Mondal, J. U.; Li, P.; Zhao, D.; Chen, B. Three-dimensional pillar-layered copper(II) metal-organic framework with immobilized functional OH groups on pore surfaces for highly selective CO<sub>2</sub>/CH<sub>4</sub> and C<sub>2</sub>H<sub>2</sub>/CH<sub>4</sub> gas sorption at room temperature. *Inorg. Chem.* **2011**, *50*, 3442–3446.
- (42) Li, J.-R.; Tao, Y.; Yu, Q.; Bu, X.-H.; Sakamoto, H.; Kitagawa, S. Selective gas adsorption and unique structural topology of a highly stable guest-free zeolite-type MOF material with N-rich chiral open channels. *Chem. - Eur. J.* **2008**, *14*, 2771–2776.
- (43) Samsonenko, D. G.; Kim, H.; Sun, Y.; Kim, G.-H.; Lee, H.-S.; Kim, K. Microporous magnesium and manganese formates for acetylene storage and separation. *Chem. - Asian J.* **2007**, *2*, 484–488.
- (44) Matsuda, R.; Kitaura, R.; Kitagawa, S.; Kubota, Y.; Belosludov, R. V.; Kobayashi, T. C.; Sakamoto, H.; Chiba, T.; Takata, M.; Kawazoe, Y.; Mita, Y. Highly controlled acetylene accommodation in a metal-organic microporous material. *Nature* **2005**, *436*, 238–241.
- (45) Mukherjee, S.; Sensharma, D.; Chen, K.-J.; Zaworotko, M. J. Crystal engineering of porous coordination networks to enable separation of C<sub>2</sub> hydrocarbons. *Chem. Commun.* **2020**, *56*, 10419–10441.
- (46) Lin, R. B.; Li, L.; Wu, H.; Arman, H.; Li, B.; Lin, R. G.; Zhou, W.; Chen, B. Optimized separation of acetylene from carbon dioxide and ethylene in a microporous material. *J. Am. Chem. Soc.* **2017**, *139*, 8022–8028.
- (47) Myers, A. L.; Prausnitz, J. M. Thermodynamics of mixed-gas adsorption. *AIChE J.* **1965**, *11*, 121–127.
- (48) Komoroski, R. A. *High resolution NMR spectroscopy of synthetic polymers in bulk*; VCH Publishers: New York, 1986.
- (49) Kolokolov, D. I.; Stepanov, A. G.; Guillerme, V.; Serre, C.; Frick, B.; Jovic, H. Probing the dynamics of the porous Zr terephthalate UiO-66 framework using <sup>2</sup>H NMR and neutron scattering. *J. Phys. Chem. C* **2012**, *116*, 12131–12136.
- (50) Schmidt, C.; Kuhn, K. J.; Spiess, H. W. Distribution of correlation times in glassy polymers from pulsed deuterium NMR. *Frontiers in Polymer Science*; Steinkopff: Darmstadt, 1985; Vol. 71, pp 71–76.
- (51) Macho, V.; Brombacher, L.; Spiess, H. W. The NMR-WEPLAB: An internet approach to NMR lineshape analysis. *Appl. Magn. Reson.* **2001**, *20*, 405–432.
- (52) Kolokolov, D. I.; Stepanov, A. G.; Jovic, H. Mobility of the 2-methylimidazole linkers in ZIF-8 probed by <sup>2</sup>H NMR: saloon doors for the guests. *J. Phys. Chem. C* **2015**, *119*, 27512–27520.
- (53) Kirstein, O.; Prager, M.; Dimeo, R. M.; Desmedt, A. Rotational dynamics of methyl groups in m-xylene. *J. Chem. Phys.* **2005**, *122*, No. 014502.
- (54) Gabuda, S. P.; Kozlova, S. G.; Samsonenko, D. G.; Dybtsev, D. N.; Fedin, V. P. Quantum rotations and chiral polarization of qubit prototype molecules in a highly porous metal-organic framework: <sup>1</sup>H NMR T<sub>1</sub> study. *J. Phys. Chem. C* **2011**, *115*, 20460–20465.
- (55) Khudozhnikov, A. E.; Arzumanov, S. S.; Kolokolov, D. I.; Kholdeeva, O. A.; Freude, D.; Stepanov, A. G. Guests like gear levers: donor binding to coordinatively unsaturated metal sites in MIL-101 controls the linker's rotation. *Chem. - Eur. J.* **2019**, *25*, S163–S168.
- (56) Zhang, Z.; Xiang, S.; Chen, B. Microporous metal-organic frameworks for acetylene storage and separation. *CrystEngComm* **2011**, *13*, S983–S992.